Dear author,

Please note that changes made in the online proofing system will be added to the article before publication but are not reflected in this PDF.

We also ask that this file not be used for submitting corrections.

Joule

CellPress

Article

Multiple Roles of a Non-fullerene Acceptor Contribute Synergistically for High-Efficiency Ternary Organic Photovoltaics

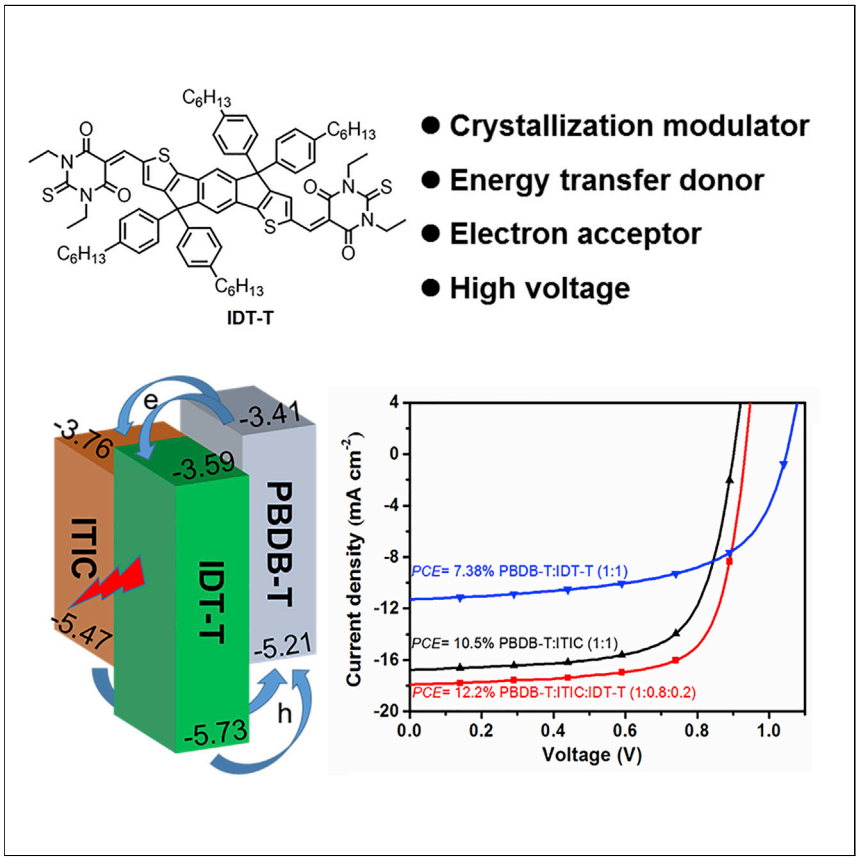

The marriage of non-fullerene acceptors (NFAs) and ternary solar cell architecture has brought about great advances in organic photovoltaics. The primary effort, however, has been focusing on low-bandgap NFAs that exploit complementary absorption and energy-level cascade. Here we report a wide-bandgap NFA IDT-T that functions as an energy-level mediator, a fluorescence resonance energy-transfer donor, an electron acceptor, and a crystallization modulator, which contribute synergistically in a ternary blend to yield high organic photovoltaic device performance.

Liangang Xiao, Bo He, Qin Hu, ..., Yong Cao, Xiaobin Peng, Yi Liu

chxbpeng@scut.edu.cn (X.P.)
yliu@lbl.gov (Y.L.)

HIGHLIGHTS

A wide-bandgap non-fullerene acceptor, IDT-T, is employed in a ternary solar cell

The ternary solar cell delivers a PCE of 12.2% with enhanced device characteristics

IDT-T transfers energy to and mediates the crystallization of another acceptor ITIC

Multiple roles of IDT-T contribute synergistically to yield high device performance

Xiao et al., Joule 2, 1–13
November 21, 2018
https://doi.org/10.1016/j.joule.2018.08.002

Please cite this article in press as: Xiao et al., Multiple Roles of a Non-fullerene Acceptor Contribute Synergistically for High-Efficiency Ternary Organic Photovoltaics, Joule (2018), https://doi.org/10.1016/j.joule.2018.08.002

Joule

CellPress

Article

Multiple Roles of a Non-fullerene Acceptor Contribute Synergistically for High-Efficiency Ternary Organic Photovoltaics

Liangang Xiao,[1,2] Bo He,[1,3] Qin Hu,[3,4] Lorenzo Maserati,[1] Yun Zhao,[1,5] Bin Yang,[6] Matthew A. Kolaczkowski,[1] Christopher A. Anderson,[1] Nicholas J. Borys,[1] Liana M. Klivansky,[1] Teresa L. Chen,[1] Adam M. Schwartzberg,[1] Thomas P. Russell,[3,4] Yong Cao,[2] Xiaobin Peng,[2,*] and Yi Liu[1,3,7,*]

SUMMARY

Ternary structure is an important design strategy to obtain high-efficiency non-fullerene organic photovoltaics (OPVs). However, the role of the third component to the standard binary system is still unclear. Here, a wide-bandgap small-molecule acceptor, denoted IDT-T, is synthesized and used together with a wide-bandgap donor polymer, PBDB-T, and a low-bandgap acceptor, ITIC, for fullerene-free ternary solar cells. The ternary cell features an enhanced power conversion efficiency (PCE) up to 12.2%, together with improved photocurrent density, open-circuit voltage (V_{OC}), and fill factor. Studies of the thin films indicate that IDT-T functions as an energy-level mediator, a fluorescence resonance energy-transfer donor, an electron acceptor, and a crystallization modulator in the blend, which contribute synergistically in the ternary blend to deliver a higher V_{OC}, more efficient exciton generation, suppressed bimolecular charge recombination and enhanced charge transport, and an overall high photovoltaic performance.

Context & Scale

Very recently, non-fullerene acceptors (NFAs) based on low-bandgap small molecules have emerged as a new class of acceptors that rival the dominance of fullerene-based acceptors. Such discovery also stimulates promising device architectures such as ternary solar cells, with a handful that have achieved high power conversion efficiencies above 12%. The primary effort, however, has been focusing on low-bandgap NFAs that exploit complementary absorption and energy-level cascade. Herein we report a rare example of a wide-bandgap NFA that leads to high-performance ternary solar cells without relying on full absorption complementarity of all three components. Detailed studies revealed the multiple roles of this acceptor in blend films, which contribute synergistically to improved device characteristics. This work may inspire new design principles of potent wide-bandgap NFAs, which will open the door to high-efficiency organic photovoltaic devices through new opportunities such as multi-component solar cells.

INTRODUCTION

The surging interest in the development of non-fullerene acceptors (NFAs) in recent years represents the latest rapid advancement in the field of organic photovoltaics (OPVs).[1–5] Single-junction devices have delivered impressive power conversion efficiencies (PCEs) and device characteristics that have already surpassed fullerene-based OPVs, due to the greater tunability of chemical structures, optical properties and electronic properties of NFAs, and their ability to phase separate into nanoscopic domains in blended thin films.[6–13] For conventional binary non-fullerene OPVs, the absorption of solar spectrum of NFAs was broadened to enhance the short-circuit current density (J_{SC}) by reducing their optical bandgaps.[14–16] Such bandgap modification is commonly accompanied by low open-circuit voltage (V_{OC}) due to the low-lying lowest unoccupied molecular orbital (LUMO) energy level in the NFA. Such a trade-off between V_{OC} and J_{SC} is an impediment in realizing the Shockley-Queisser theoretical maximum efficiency in non-fullerene OPVs.[17,18] Ternary solar cells using a third component in the active layer offer a mix-and-match solution to realize a desirable energy-level cascade and complementary absorption, and has emerged as a promising device architecture to achieve high efficiencies.[19–27] Several common design criteria have been conceived and exercised to improve charge generation and collection efficiencies in ternary OPVs,

Please cite this article in press as: Xiao et al., Multiple Roles of a Non-fullerene Acceptor Contribute Synergistically for High-Efficiency Ternary Organic Photovoltaics, Joule (2018), https://doi.org/10.1016/j.joule.2018.08.002

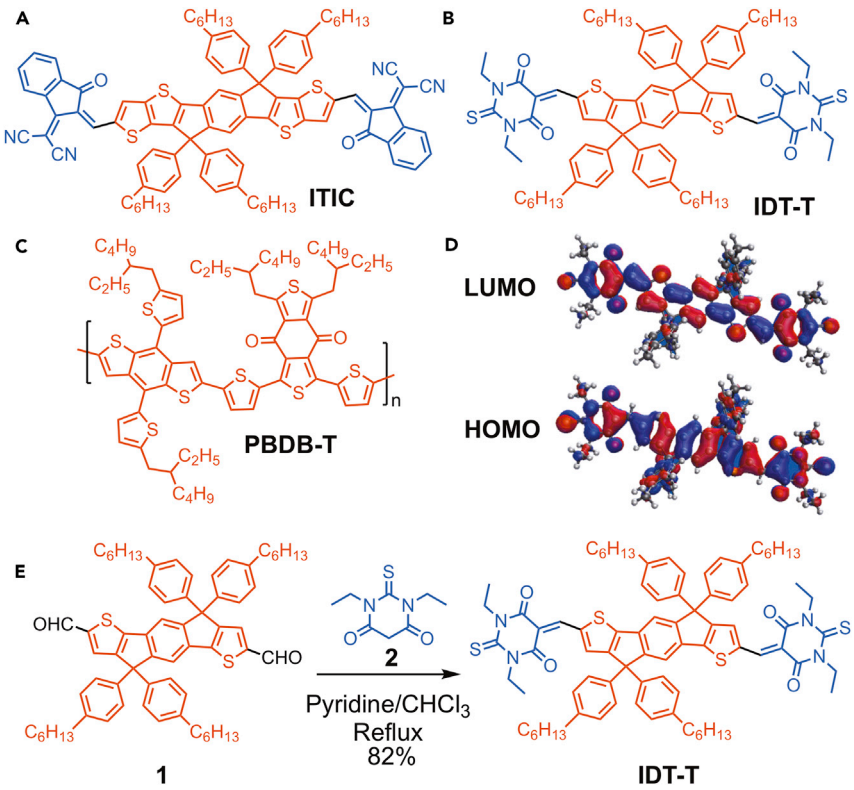

Q9 Scheme 1.

Chemical structures of (A) ITIC, (B) IDT-T, and (C) PBDB-T.
(D) Frontier molecular orbital plots of IDT-T.
(E) The synthetic scheme of IDT-T.

which typically concern the fulfillment of complementary absorption, modulation of V_{OC} to circumvent energy-level pinning to the smaller value of the two binary solar cells, and good miscibility amid all the components for optimal film morphology. Building on the early success whereby two donors and one fullerene acceptor were used as the active components,[28–33] non-fullerene-based ternary solar cells have progressed rapidly,[16,34–41] although only a few are able to deliver PCEs over 12%. Recently Hou and co-workers reported the use of one wide-bandgap polymer donor and two low-bandgap NFAs to achieve solar cells with a PCE of 11.1%.[42] Solar cells with a PCE of 12.16% were also realized by Ge and co-workers using one mid-gap polymer together with one wide-gap NFA and one low-bandgap NFA.[43] Peng and co-workers employed two energy-transfer donor polymers and a wide-gap NFA in ternary solar cells to realize an efficiency of 12.27%.[15]

One representative class of NFAs is ITIC (5,5,11,11-tetrakis(4-hexylphenyl)-dithieno[2,3-d:2′,3′-d′]-s-indaceno[1,2-b:5,6-b′]dithiophene; Scheme 1A) and its analogs,[44–46] the relatively low-lying LUMO energy levels of which typically result in low V_{OC} in the corresponding solar cells. Raising the LUMO energy levels of the electron acceptor can increase the V_{OC} in either a binary solar cell or a ternary cell if the V_{OC} scales with the increasing fraction of the acceptor with a higher LUMO energy level. Based on the acceptor-donor-acceptor structural feature of ITIC, energy-level tuning can be implemented by changing the central fused ring system, introducing a π bridge between the donor and acceptor moieties, and/or using end groups with

[1]The Molecular Foundry, Lawrence Berkeley National Laboratory, Berkeley, CA 94720, USA

[2]Institute of Polymer Optoelectronic Materials and Devices, State Key Laboratory of Luminescent Materials and Devices, South China University of Technology, 381 Wushan Road, Guangzhou 510640, P.R. China

[3]Materials Sciences Division, Lawrence Berkeley National Lab, Berkeley, CA 94720, USA

[4]Polymer Science and Engineering Department, University of Massachusetts, Amherst, MA 01003, USA

[5]School of Chemical Engineering and Technology, China University of Mining and Technology, Xuzhou 221116, China

[6]College of Materials Science and Engineering, Key Laboratory for Micro-Nano Physics and Technology of Hunan Province, Hunan University, Changsha 410082, China

[7]Lead Contact

*Correspondence: chxbpeng@scut.edu.cn (X.P.), yliu@lbl.gov (Y.L.)

https://doi.org/10.1016/j.joule.2018.08.002

Please cite this article in press as: Xiao et al., Multiple Roles of a Non-fullerene Acceptor Contribute Synergistically for High-Efficiency Ternary Organic Photovoltaics, Joule (2018), https://doi.org/10.1016/j.joule.2018.08.002

different electron-accepting abilities. The most common end groups are rhodanine units or malononitrile-derived indanone variants that possess differential electron-withdrawing ability.[46–49] Herein, to further raise the LUMO energy level and decrease the highest occupied molecular orbital (HOMO) energy level, a weakly electron-withdrawing thiobarbituric acid (TBA) unit[50,51] is employed as the end group for coupling with a penta-fused indacenodithiophene (IDT) core to afford a wide-bandgap NFA acceptor, IDT-T (Scheme 1B). We have demonstrated that IDT-T and ITIC are efficient fluorescence resonance energy transfer (FRET) partners[52–55] that display both spectroscopic complementarity and great miscibility in the blended film. Spectroscopic studies provided great details of energy-transfer and electron-transfer processes in the ternary blend involving a mid-bandgap polymer donor, PBDB-T (Scheme 1C) and the two acceptors, while grazing incidence wide-angle X-ray scattering (GIWAXS) studies revealed a unique composition-dependent crystallization behavior. The well-aligned molecular orbitals and good spectrum complementarity, together with combined electron-transfer and energy-transfer processes in the optimally intermixed three-component blends, lead to ternary organic solar cells (OSCs) with a high PCE of 12.2%, a V_{OC} of 0.935 V, a J_{SC} of 17.9 mA cm^{-2}, and a high fill factor (FF) of 73.1%. These device parameters are significantly enhanced compared with the corresponding PBDB-T:ITIC binary device, attributable to the unique roles of the IDT-T acceptor that incurs higher V_{OC}, greater exciton generation, suppressed charge recombination, and enhanced charge transport.

RESULTS AND DISCUSSION

Molecular modeling of IDT-T based on density function theory calculations indicated a 0.11-eV increase and 0.22-eV decrease of the LUMO and HOMO energy levels compared with that of ITIC, respectively, corresponding to a 0.33-eV increase of the optical bandgap (Table S1). The frontier molecular orbital plots (Scheme 1D) illustrate that both HOMO and LUMO are effectively delocalized across the core and the end groups. IDT-T was synthesized in 82% yield from the Knoevenagel condensation reaction between bisaldehyde (**1**) and thiobarbituric acid (**2**) (Scheme 1E and Supplemental Experimental Procedures). UV-visible studies of IDT-T in tetrahydrofuran (Figure S2) indicate a red-shift of 25 nm in comparison with its thin-film absorption (Figure 1A), suggesting intermolecular π-π stacking in the solid state. Due to the decreased effective conjugated length and the weaker electron-withdrawing properties of the end groups, IDT-T shows a significantly blue-shifted optical absorption when compared with ITIC. As shown in Figure 1A, IDT-T has an absorption maximum and edge at 608 nm and 650 nm, respectively, in contrast to 705 nm and 800 nm for ITIC, clearly showing their complementary absorption features. The optical bandgap (E_g^{opt}) of IDT-T calculated from the onset of film absorption is 1.91 eV, 0.36 eV larger than that of ITIC. On the other hand, strong overlap between the absorption spectra of IDT-T and PBDB-T in the range of 500–650 nm is observed. Notably, IDT-T has a higher extinction coefficient (1.26×10^5 cm^{-1}) than PBDB-T (5.49×10^4 cm^{-1}) and ITIC (1.05×10^5 cm^{-1}), underlining its strong absorbing property. The absorption spectra of ternary-blend films with constant 1:1 donor/acceptor ratio but varying IDT-T compositions (Figure S3) show that increasing the fraction of IDT-T gradually increases the absorption intensity between 500 and 630 nm, together with a decrease in the absorption intensity between 650 and 750 nm due to the diminished contribution from ITIC. The LUMO and HOMO levels are evaluated using electrochemical methods (Figure S1A), which are estimated to be −3.59 eV and −5.73 eV for IDT-T and −3.76 eV and −5.47 eV for ITIC, respectively. The HOMO-LUMO energy gaps and the relative energy-level

Please cite this article in press as: Xiao et al., Multiple Roles of a Non-fullerene Acceptor Contribute Synergistically for High-Efficiency Ternary Organic Photovoltaics, Joule (2018), https://doi.org/10.1016/j.joule.2018.08.002

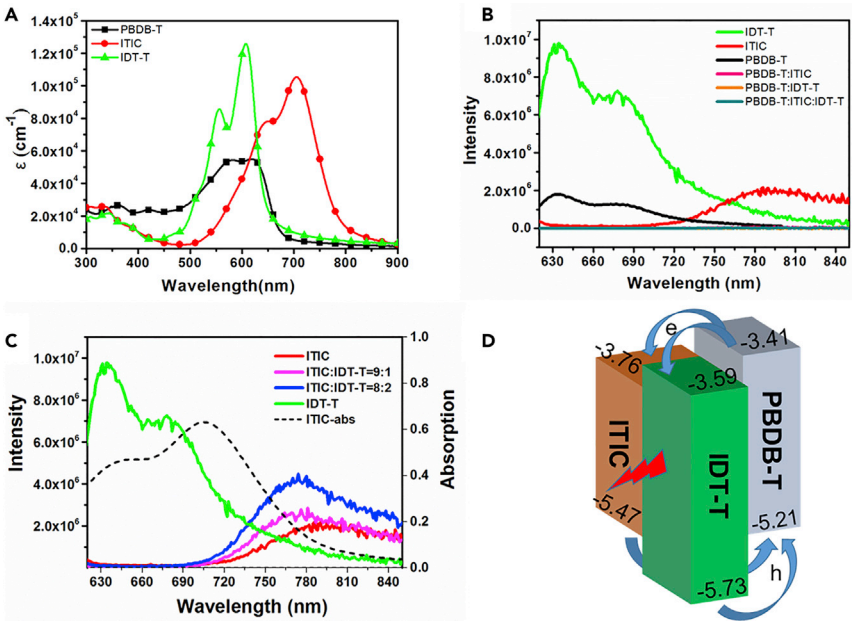

Figure 1. UV-Visible and Fluorescence Spectra of Single Component or Mixtures of PBDB-T, ITIC, and IDT-T, and Their Related Energy Diagram

(A) UV-visible absorption spectra of PBDB-T, ITIC, and IDT-T in films.

(B) PL spectra of PBDB-T, ITIC, and IDT-T, and the corresponding donor-acceptor binary and ternary blends. Note that all of the spectra of the blends are at the baselines.

(C) PL spectra of ITIC, IDT-T, and their mixtures at the weight ratios of 9:1 and 8:2. The excitation wavelength is 608 nm. The UV-visible spectrum of ITIC is also plotted (dotted line) to show the good overlap with PL spectra of IDT-T.

(D) Schematic energy diagram of PBDB-T, ITIC, and IDT-T, and the related electron and energy-transfer processes.

alignment are consistent with optical measurements and theoretical calculations (Table S1).

To understand the photoexcitation and related processes in the multi-component donor-acceptor systems, we measured photoluminescence (PL) spectra of films of individual components and those with different compositions with excitation at 608 nm. As shown in Figure 1B, the PL of all the components is effectively quenched in both the binary and ternary donor/acceptor blend films, suggesting efficient charge transfer between the donor and acceptor(s) in these films. In contrast, the binary blend of ITIC and IDT-T has PL behavior characteristic of FRET. The broad emission between 620 and 700 nm of the pure IDT-T thin film disappeared in the PL spectrum of the 9:1 mixture of ITIC:IDT-T, concomitant with a broad ITIC emission between 720 and 840 nm. Increasing the IDT-T weight ratio to 20 wt% does not result in emission from IDT-T itself but instead induces stronger ITIC emission. Such emission properties suggest that IDT-T and ITIC behave as a donor and acceptor FRET pair, which is consistent with the large overlap between the emission spectrum of IDT-T and the absorption spectrum of ITIC (Figures 1C and S4). The efficient energy transfer also implies that IDT-T and ITIC molecules are well mixed and closely packed (within 10 nm) for effective non-radiative energy transfer.[56,57] This good miscibility between electron acceptors is conducive to the formation of a nanoscopic phase separation needed to realize high FF. The non-radiative energy transfer from IDT-T and ITIC also enables generation of extra ITIC excitons, which, when combined with the efficient electron transfer between

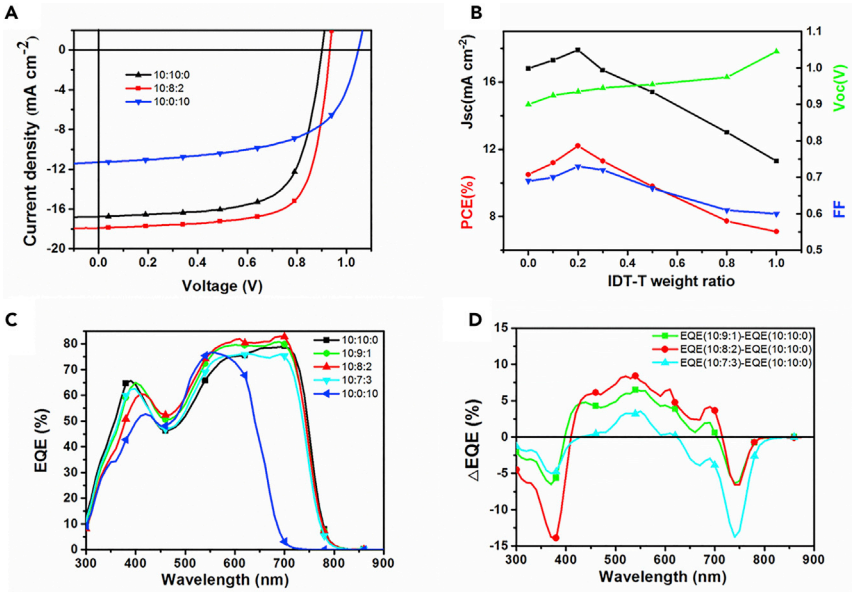

Figure 2. Device Characteristics and EQE Plots of the OPV Devices

(A) Representative *J-V* curves of two binary solar cells and the best-performing ternary solar cell.

(B) Plot of J_{SC}, V_{OC}, FF, and PCE values at different IDT-T weight ratios. The black represents J_{SC}, the red line PCE, the green line V_{OC}, and the blue line FF.

(C) EQE curves of ternary solar cell devices based on different weight ratios.

(D) Difference in EQE spectra. The legends indicate weight ratios of PBDB-T:ITIC:IDT-T.

the donor and acceptors, may offer a unique pathway to produce high photocurrent in ternary blends.

OSC devices were fabricated with a structure of ITO/ZnO/active layer/MoO_3/Al to evaluate the photovoltaic performances of the binary and ternary mixtures. The *J-V* curves of the best-performing devices are shown in Figure 2A. The optimal binary solar cell devices based on PBDB-T and IDT-T show a moderate PCE of 7.40% and an impressive V_{OC} of 1.05 V (Figure 2A; Tables 1, S2, and S3), which can be associated with the large energy-level separation between the high-lying LUMO energy level of IDT-T and the HOMO of PBDT-T. The binary solar cells based on PBDB-T:ITIC exhibit a PCE of 10.5%, an efficiency that is comparable with that in previous reports,[58–60] with a J_{SC} of 16.80 mA cm^{-2}, a V_{OC} of 0.900 V, and an FF of 0.69.

Ternary solar cells were fabricated where the IDT-T:ITIC ratios were systematically varied while keeping the overall donor/acceptor ratio at 1:1. The best-performing ternary OSC devices were obtained at the weight ratio of 1:0.8:0.2 for PBDB-T:ITIC:IDT-T, showing an average PCE of 12.0% and a maximum PCE of 12.2% with a J_{SC} of 17.9 mA cm^{-2}, a V_{OC} of 0.935 V, and an FF of 73.1% (Figures 2A and S5). The simultaneous improvement of all three parameters leads to a 17% enhancement in PCE compared with the corresponding binary solar cells based on PBDB-T:ITIC. Respectful PCEs higher than 11% were maintained when the weight percentage of IDT-T in the acceptors was kept at less than 50 wt% (Figure 2B and Table 1). The J_{SC} of the devices increased to 17.9 mA cm^{-2} when 20 wt% IDT-T was employed and decreased to 13.0 mA cm^{-2} at 80 wt% IDT-T. Meanwhile, the FFs of the devices also increased from 69.3% to 73.1% at 20 wt% loading of IDT-T and reduced to 61.0% at 80 wt% IDT-T. In contrast to the trends in J_{SC} and FF changes, increasing the fraction of IDT-T results in monotonically increased V_{OC}

Please cite this article in press as: Xiao et al., Multiple Roles of a Non-fullerene Acceptor Contribute Synergistically for High-Efficiency Ternary Organic Photovoltaics, Joule (2018), https://doi.org/10.1016/j.joule.2018.08.002

Table 1. Photovoltaic Parameters for PBDB-T:ITIC:IDT-T-Based Solar Cells with Different Weight Ratios of IDT-T

PBDB-T:ITIC:IDT-T	J_{SC} (mA cm^{-2})	V_{OC} (V)	FF (%)	PCE (%)
1:1:0	16.8 (16.3)[a]	0.900	69.3	10.5[b] (10.4 ± 0.2)[c]
1:0.9:0.1	17.3 (16.8)[a]	0.920	70.5	11.2[b] (11.1 ± 0.1)[c]
1:0.8:0.2	17.9 (17.3)[a]	0.935	73.1	12.2[b] (12.0 ± 0.2)[c]
1:0.7:0.3	16.7 (16.2)[a]	0.945	72.0	11.4[b] (11.1 ± 0.2)[c]
1:0.5:0.5	15.3 (14.7)[a]	0.955	67.2	9.82[b] (9.68 ± 0.16)[c]
1:0.2:0.8	13.0 (12.6)[a]	0.975	61.0	7.74[b] (7.51 ± 0.14)[c]
1:0:1	11.8 (11.3)[a]	1.05	59.8	7.38[b] (7.25 ± 0.14)[c]

[a]J_{SC} calculated from EQE curves.
[b]The best PCE.
[c]Average PCE from ten devices.

(Figure 2B). The compositional dependence of V_{OC} in ternary-blend solar cells suggests that photoinduced charges are collected by separate charge-transfer paths involving IDT-T and ITIC without energy-level pinning.

The external quantum efficiencies (EQEs) of the PBDB-T:ITIC:IDT-T ternary solar cells were measured and are plotted in Figure 2C and S6. The device based on PBDB-T:ITIC exhibits a broad EQE response extending into the 800-nm region, while the EQE response of the PBDB-T:IDT-T binary device mainly falls within the range between 500 and 700 nm, together with notably lower quantum efficiencies. As shown in the difference EQE plot in Figure 2D, incorporating 10 wt% IDT-T as the third component into the solar cell significantly enhances the EQE values in the region between 500 and 650 nm, accompanied by decreased EQE in the region between 710 and 800 nm, which are consistent with the absorptivity of IDT-T in these ranges. Intriguingly, simultaneous enhancement of EQE was also observed in the region between 650 and 720 nm, where decreased absorption is expected due to the limited absorption range of IDT-T and lower fraction of ITIC in the blend. At 20 wt% IDT-T, the quantum efficiency in the 500- to 800-nm region rises further while the dip at 745 nm remains at a similar level. Further increase of IDT-T fraction in the ternary-blend system leads to significantly reduced EQEs. The overall EQE dependence on acceptor compositions is fully consistent with the corresponding device performances. In addition, the calculated J_{SC} from the EQE measurement is slightly lower (less than 5%) but still in good agreement with the J_{SC} obtained from the *J-V* measurements, which confirms high consistency of the photovoltaic results. The apparent inverse correlation between the EQE enhancement and the decreased light absorption in the long-wavelength region suggests processes other than direct photoexcitation that compensate the absorption loss to afford an overall increased photocurrent.

Both transient absorption (TA) measurements and time-resolved photoluminescence (TR-PL) studies were carried out to provide more insight into the involved charge-transfer and energy-transfer processes. We found that TA measurement convincingly revealed improved hole transfer within the blends while TR-PL was more suitable to probe the FRET process. In the TA studies, to simplify the investigation of charge carriers' dynamics in the blends, we chose to excite the materials at the lowest transition, i.e., the HOMO-LUMO of ITIC (710 nm). This allowed us to selectively excite a single component while monitoring the spectral dynamics of the entire system. Figure 3A shows a comparison of the 625- to 635-nm integrated spectral range in the ITIC, ITIC:PBDB-T (1:1), and ITIC:IDT-T:PBDB-T (8:2:10) films.

Please cite this article in press as: Xiao et al., Multiple Roles of a Non-fullerene Acceptor Contribute Synergistically for High-Efficiency Ternary Organic Photovoltaics, Joule (2018), https://doi.org/10.1016/j.joule.2018.08.002

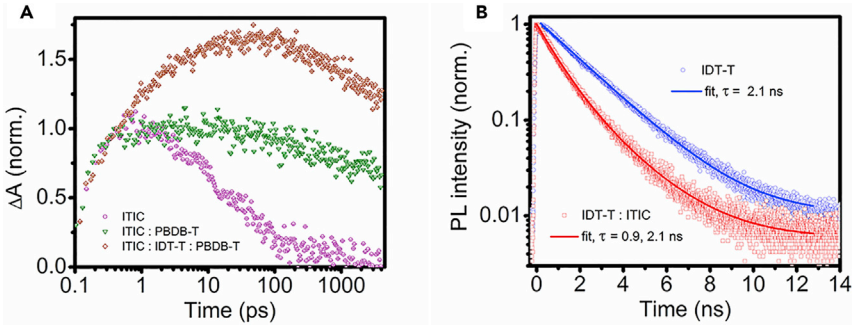

Figure 3. Transient Absorption and TR-PL Spectra of the Donor and Acceptors

(A) Transient absorption spectroscopy on ITIC (purple circles), ITIC:PBDB-T (green triangles), and ITIC:IDT-T:PBDB-T (brown diamonds) films. The films are pumped with a 50-fs pulse at 710 nm (fluence 32 μJ cm^{-2}), probed in the range 625–635 nm, and averaged data in that range are plotted. The differential absorption signals are normalized to 1 at the time when the pump pulse peaks. The further rise of the signals in the blends is associated with the hole injection in the PBDB-T and the consequent bleaching of its 630-nm transition. A more significant hole injection is observed in the three-component blend.

(B) Time-resolved photoluminescence of IDT-T (blue circles) and ITIC:IDT-T (red squares). The films are pumped with a 5-ps pulse at 517 nm (fluence 200 μJ cm^{-2}) and the PL is collected in the range 532–600 nm corresponding to the IDT-T emission line. The PL lifetime decays significantly faster in the blend due to an additional decay channel with a 0.9-ns exponential time constant, suggesting an energy transfer from IDT-T to ITIC.

For the sake of comparison, the data are normalized at the pump pulse peak. In the pure ITIC thin film a transition bleaching is observed, corresponding to the transition from the HOMO to the second-lowest unoccupied molecular orbital. When ITIC is blended with the donor (PBDB-T), the creation of exciton due to resonant optical pumping is immediately followed by a hole transfer to the PBDB-T HOMO. This depopulation of ground state of the donor causes a bleach in its two optical transitions (570 and 630 nm) that we observe as an increase in the absolute value of the differential absorption signal in that spectral range for several picoseconds after the pulse. The intensity of this differential absorption is such that the ITIC bleaching signal is completely swallowed. This same effect is present and significantly more pronounced in the three-component blend, where the hole injection appears more efficient and clearly visible on a longer timescale (up to 100 ps), even though the IDT-T is not excited. The hole injection signal increased in both intensity and duration when going from the binary to the ternary blend, which clearly suggested that the presence of IDT-T does not block the hole transfer but instead improves it. This enhanced hole transfer may be related to the FRET process from IDT-T to ITIC occurring in the ternary blend, which creates additional holes in ITIC that will be subsequently injected into PBDB-T. The longer hole-transfer timescale may also be related to the formation of co-crystallized acceptor domains (see later discussion on the morphological studies) where holes are more delocalized, which correlates well with the larger J_{SC} observed in devices.

On the other hand, the steady-state PL already suggested an FRET process involving the IDT-T and the ITIC molecules. TR-PL studies confirmed that this effect happens when we directly excite the IDT-T HOMO-LUMO transition in the IDT-T:ITIC (2:8) blend film. Figure 3B shows a comparison between the PL of the blend and that of the pure IDT-T film. In the blend, an additional decay channel is present (represented by an additional, faster time constant of 0.9 ns). This leads to the conclusion that 70% (relative amplitude of the fast decay, see Table S4) of the excited molecular orbitals undergo FRET. Since this effect happens on the nanosecond timescale, it will sum up

Please cite this article in press as: Xiao et al., Multiple Roles of a Non-fullerene Acceptor Contribute Synergistically for High-Efficiency Ternary Organic Photovoltaics, Joule (2018), https://doi.org/10.1016/j.joule.2018.08.002

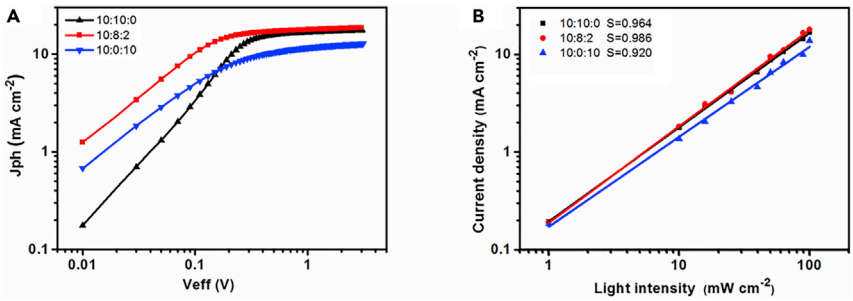

Figure 4. Dependence of Photocurrent Density on Effective Voltages and Light Intensity

(A) Photocurrent density versus effective voltage curves of solar cells based on different IDT-T weight ratios.

(B) Dependence of J_{SC} on light intensity for the solar cells based on different IDT-T weight ratio. The legends indicate weight ratios of PBDB-T:ITIC:IDT-T.

to the subnanosecond charge transfer discussed above, contributing to an overall increased hole transfer from the ITIC to the PBDB-T in the three-component blend under solar cell working conditions.

Single-carrier devices were fabricated and the dark *J-V* curves measured to evaluate the carrier mobilities using the space-charge limited current method[61] (Figures S7A and S7B). The hole and electron mobilities are 2.82×10^{-4} and 1.88×10^{-4} $cm^2\ V^{-1}\ s^{-1}$ for the binary PBDB-T:ITIC-based device, and 2.17×10^{-4} and 7.68×10^{-5} $cm^2\ V^{-1}\ s^{-1}$ for the binary PBDB-T:IDT-T-based device, respectively. The respective hole and electron mobilities are 3.17×10^{-4} and 1.97×10^{-4} $cm^2\ V^{-1}\ s^{-1}$ for the optimal ternary solar cells. The simultaneously enhanced hole and electron mobilities correlate well with the improvement of FF. To gain insight into exciton dissociation and charge-collection efficiency of ternary solar cells with different IDT-T weight ratios, we plotted photocurrent density (J_{ph}) against the effective voltage (V_{eff}) of the cells. J_{ph} and V_{eff} are defined by the following equations:

$$J_{ph} = J_L - J_D, \quad \text{(Equation 1)}$$

$$V_{eff} = V_o - V_a, \quad \text{(Equation 2)}$$

where J_L and J_D are the current densities under illumination and in the dark, respectively; V_o is the voltage at $J_{ph} = 0$; and V_a is the applied voltage.[62,63]

As shown in Figure 4A, J_{ph} is linearly proportional to the voltage at low V_{eff} and reaches saturation (J_{sat}) when V_{eff} is over 2 V, where charge recombination is minimized due to the high internal electric field in the solar cells. The charge dissociation and collection probability P(E,T) of the solar cell devices, which can be assessed by the J_{ph}/J_{sat} ratio under short-circuit conditions, are 96.5%, 97.2%, and 93.1% for PBDB-T:ITIC:IDT-T compositions at 10:10:0, 10:8:2, and 10:0:10, respectively. The larger P(E,T) of the ternary solar cell compared with the PBDB-T:ITIC binary solar cell indicates that the ternary blend facilitates a higher charge dissociation rate, which is conducive for enhanced J_{SC} and FF. Furthermore, the maximum exciton generation rate (G_{max}) of the solar cells was calculated based on the equation $J_{sat} = qLG_{max}$, where q is elementary charge, L is the thickness of the active layer, and J_{sat} is the J_{ph} at a high V_{eff} of 2 V, under which conditions J_{sat} is only limited by G_{max} since all the photogenerated excitons are dissociated into free charge carriers. The values for the three devices are 1.07×10^{28} $m^{-3}\ s^{-1}$, 1.15×10^{28} $m^{-3}\ s^{-1}$, and 7.92×10^{27} $m^{-3}\ s^{-1}$ for PBDB-T:ITIC:IDT-T compositions at 10:10:0, 10:8:2, and 10:0:10, respectively. The higher G_{max} in ternary solar cells indicates increased

Please cite this article in press as: Xiao et al., Multiple Roles of a Non-fullerene Acceptor Contribute Synergistically for High-Efficiency Ternary Organic Photovoltaics, Joule (2018), https://doi.org/10.1016/j.joule.2018.08.002

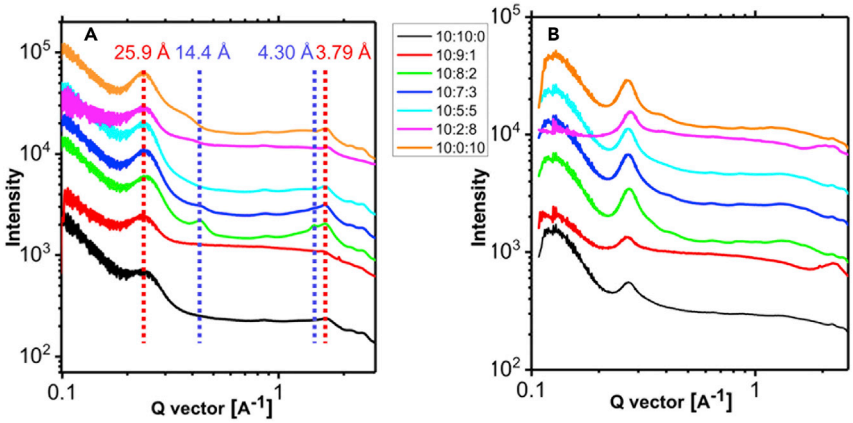

Figure 5. Linecuts of the GIWAXS Patterns of the Blends

(A and B) Vertical linecuts (A) and horizontal linecuts (B) of the GIWAXS patterns of the blends at different mixing ratios of PBDB-T:ITIC:IDT-T. The dotted red and blue lines are eye guides that indicate the two sets of peaks from PBDB-T and the induced crystallites, respectively.

overall exciton generation after adding 20 wt% IDT-T, which correlates well with the complementary absorption between IDT-T and ITIC, higher absorption coefficient of IDT-T compared with polymer PBDB-T, and sensitization of ITIC via energy transfer from IDT-T.

To further investigate the effect of dual acceptors on the charge recombination of the solar cell devices, we measured J_{SC} of solar cells based on three different compositions as a function of light intensity (P_{light}). Generally, J_{SC} shows a power-law dependence on light intensity, which can be expressed as $J_{SC} \propto (P_{light})^S$, where P_{light} is light intensity and S is the exponential factor. Completely suppressed bimolecular recombination in a device would lead to an S value equal to 1.[64,65] As shown in Figure 4B, the S values are 0.964, 0.986, and 0.920 for devices with PBDB-T:ITIC:IDT-T compositions at 10:10:0, 10:8:2, and 10:0:10, respectively. The highest S value of the three-component device indicated that the bimolecular recombination was effectively suppressed after adding 20 wt% IDT-T, consistent with the observed higher J_{SC} and FF.

Atomic force microscopy studies of blend films with different weight ratios of IDT-T show that all the films have smooth surfaces (Figure S8). The root-mean-square roughness is typically under 1.8 nm with the exception of the film with 80 wt% IDT-T, which has a slightly higher roughness of 2.7 nm. All the thin films exhibit discernible interpenetrated fibril networks that are conducive for charge transport. GIWAXS patterns of the blends shown in Figure S9 and the out-of-plane line cut (Figure 5A) show reflection at *d* spacing of 3.79 Å arising from the π-π stacking of adjacent chains. The reflection is highly oriented in the out-of-plane direction, barely evident in the in-plane line cut (Figure 5B), indicating that the chains assume a face-on orientation. Additional reflections in the out-of-plane direction are seen at *d* spacings of 14.4 Å and 4.30 Å for films containing 20 wt% and 30 wt% IDT-T, with the 20 wt% IDT-T film showing a greater intensity. As indicated by the blue dotted lines in Figure 5A, these reflections are independent of the lamellar stacking peak of the donor, seen at *d* spacing of 25.9 Å, and the π-stacking peak at *d* spacing of 3.79 Å. As can be seen from the GIWAXS profiles of pure ITIC and IDT-T (Figure S10), ITIC displays out-of-plane peaks at *d* spacings of 11.1 Å and 4.05 Å, and for IDT-T similar peaks are observed at slightly larger *d* spacings of 20.3 Å and

4.91 Å. The *d* spacings of 14.4 Å and 4.30 Å in the ternary blends are between these from pure ITIC and IDT-T, which suggest the co-crystallization of the two acceptors at an intermediate periodicity. The absence of these scattering peaks in the blends at other compositions also suggests that the co-crystallization of ITIC and IDT-T occurs only under specific conditions within the confined geometry of the acceptor phase. Resonance soft X-ray scattering (RSoXS) shows an interference at ~62 nm, characteristic of center-to-center separation distance between domains (Figure S11) for all the blend films. Consequently, the picture of the morphology that arises from all of these data is one nanoscopic crystalline fibril of the acceptor embedded in a matrix of the donor that assumes a face-on orientation. The co-crystallites of ITIC and IDT-T formed within the acceptor domains at 20 wt% and 30 wt% IDT-T loading correlate well with the peak device performances at these compositions. We are not aware of observations of this co-crystallization behavior in other ternary systems, and from the performance results this may point to a key morphology feature to enhance performance.

In summary, an electron acceptor, IDT-T, was synthesized and used in high-efficiency ternary OPVs. IDT-T features a penta-fused aromatic central moiety and two weakly withdrawing TBA end groups, which has a wide bandgap of 1.91 eV, a high extinction coefficient, and a high-lying LUMO energy level. The ternary OPV devices employing PBDB-T:ITIC:IDT-T at the composition of 10:8:2 display a highest efficiency of 12.2%, with a J_{SC} of 17.9 mA cm^{-2}, a V_{OC} of 0.935 V, and an FF of 73.1%, all being significantly higher than the corresponding binary PBDB-T:ITIC device. The addition of IDT-T contributes to the increased EQE not only in shorter-wavelength region where it has strong absorption but also in the longer-wavelength region where absorption is diminished. Such EQE enhancement correlates with improved hole transfer in the three-component blend observed by TA measurements and energy-transfer process from IDT-T to ITIC verified by TR-PL spectroscopy. Notably, the structural similarity between ITIC and IDT-T permits great miscibility in the thin film, which not only facilitates efficient energy transfer but also induces crystallization of the acceptors. While the reported PCE here is among the highest-performing ternary solar cells (see Table S5 for a performance comparison), it constitutes a rare example that does not rely on full absorption complementarity of all three components.[41] The high efficiency of the ternary solar cells highlights the multiple roles of IDT-T: an energy-level mediator, an energy-transfer donor, an electron acceptor, and a solid-state crystallization modulator, which contribute synergistically to higher V_{OC}, J_{SC}, and FF in the corresponding devices.

EXPERIMENTAL PROCEDURES

Full details of experiments are provided in Supplemental Experimental Procedures.

SUPPLEMENTAL INFORMATION

Supplemental Information includes Supplemental Experimental Procedures, 11 figures, and 5 tables and can be found with this article online at https://doi.org/10.1016/j.joule.2018.08.002.

ACKNOWLEDGMENTS

Q11 Part of this work was performed as a user project at the Molecular Foundry, and the X-ray experiments were conducted at the Advanced Light Source, Lawrence Berkeley National Laboratory, all supported by the Office of Science, Office of Basic Energy Sciences, of the U.S. Department of Energy under contract no. DE-AC02-05CH11231. This work was also supported by the U.S. Department of Energy, Office

of Science, Office of Basic Energy Sciences, Materials Sciences and Engineering Division, under contract no. DE-AC02-05-CH11231 within the Inorganic/Organic Nanocomposites Program (KC3104) (B.H. and Y.L. for materials design, synthesis, and analysis). X.P. acknowledges financial support from the National Key Research and Development Program of China (2017YFA0206602) and the National Natural Science Foundation of China (51773065, 51473053). L.X. acknowledges support from Chinese Scholar Counsel. Q.H. and T.P.R. were supported by the Office of Naval Research, Materials Division, under contract no. N00014-17-1-2241.

AUTHOR CONTRIBUTIONS

Y.L. proposed the research, directed the study, and analyzed the data. L.X. carried out the device fabrication and characterizations and analyzed the data. B.H. prepared the material of IDT-T. Q.H. helped with RSoXS measurement. L.M., A.M.S., and N.J.B. carried out TA and TR-PL measurements. M.A.K. and C.A.A. helped with materials characterization. B.Y., Y.Z., T.L.C., and L.M.K. helped with device fabrication and characterization. Y.L. and L.X. prepared the manuscript. X.P. and Y.L. supervised the whole project. All authors (L.X., B.H., Q.H., L.H., Y.Z., B.Y., M.A.K., C.A.A., N.J.B., L.M.K., T.L.C., A.M.S., T.P.R., Y.C., X.P., and Y.L.) discussed Q10 the results and commented on the manuscript.

DECLARATION OF INTERESTS

The authors declare no competing interests.

Received: June 28, 2018
Revised: July 18, 2018
Accepted: August 8, 2018
Published: August 31, 2018

REFERENCES

1. Hou, J.H., Inganas, O., Friend, R.H., and Gao, F. (2018). Organic solar cells based on non-fullerene acceptors. Nat. Mater. *17*, 119–128.

2. Yan, C., Barlow, S., Wang, Z., Yan, H., Jen, A.K.Y., Marder, S.R., and Zhan, X. (2018). Non-fullerene acceptors for organic solar cells. Nat. Rev. Mater. *3*, 18003–18021.

3. Cheng, P., Li, G., Zhan, X., and Yang, Y. (2018). Next-generation organic photovoltaics based on non-fullerene acceptors. Nat. Photonics *12*, 131–142.

4. Sun, C., Xia, R., Shi, H., Yao, H., Liu, X., Hou, J., Huang, F., Yip, H.-L., and Cao, Y. (2018). Heat-insulating multifunctional semitransparent polymer solar cells. Joule *2*, https://doi.org/10.1016/j.joule.2018.06.006.

5. Chang, S.-Y., Cheng, P., Li, G., and Yang, Y. (2018). Transparent polymer photovoltaics for solar energy harvesting and beyond. Joule *2*, 1039–1054.

6. Xiao, Z., Jia, X., Li, D., Wang, S.Z., Geng, X.J., Liu, F., Chen, J.W., Yang, S.F., Russell, T.P., and Ding, L.M. (2017). 26 mA cm(-2) J(sc) from organic solar cells with a low-bandgap nonfullerene acceptor. Sci. Bull. *62*, 1494–1496.

7. Fan, B.B., Ying, L., Zhu, P., Pan, F.L., Liu, F., Chen, J.W., Huang, F., and Cao, Y. (2017). All-polymer solar cells based on a conjugated polymer containing siloxane-functionalized side chains with efficiency over 10%. Adv. Mater. *29*, 1703906–1703912.

8. Zhao, W.C., Li, S.S., Yao, H.F., Zhang, S.Q., Zhang, Y., Yang, B., and Hou, J.H. (2017). Molecular optimization enables over 13% efficiency in organic solar cells. J. Am. Chem. Soc. *139*, 7148–7151.

9. Li, Y.X., Lin, J.D., Che, X.Z., Qu, Y., Liu, F., Liao, L.S., and Forrest, S.R. (2017). High efficiency near-infrared and semitransparent non-fullerene acceptor organic photovoltaic cells. J. Am. Chem. Soc. *139*, 17114–17119.

10. Song, X., Gasparini, N., Ye, L., Yao, H., Hou, J., Ade, H., and Baran, D. (2018). Controlling blend morphology for ultrahigh current density in nonfullerene acceptor-based organic solar cells. ACS Energy Lett. *3*, 669–676.

11. Zhang, A.D., Li, C., Yang, F., Zhang, J.Q., Wang, Z.H., Wei, Z.X., and Li, W.W. (2017). An electron acceptor with porphyrin and perylene bisimides for efficient non-fullerene solar cells. Angew. Chem. Int. Ed. *56*, 2694–2698.

12. Li, Y.X., Zhong, L., Gautam, B., Bin, H.J., Lin, J.D., Wu, F.P., Zhang, Z.J., Jiang, Z.Q., Zhang, Z.G., Gundogdu, K., et al. (2017). A near-infrared non-fullerene electron acceptor for high performance polymer solar cells. Energy Environ. Sci. *10*, 1610–1620.

13. Li, S.S., Ye, L., Zhao, W.C., Zhang, S.Q., Mukherjee, S., Ade, H., and Hou, J.H. (2016). Energy-level modulation of small-molecule electron acceptors to achieve over 12% efficiency in polymer solar cells. Adv. Mater. *28*, 9423–9429.

14. Baran, D., Ashraf, R.S., Hanifi, D.A., Abdelsamie, M., Gasparini, N., Röhr, J.A., Holliday, S., Wadsworth, A., Lockett, S., Neophytou, M., et al. (2016). Reducing the efficiency-stability-cost gap of organic photovoltaics with highly efficient and stable small molecule acceptor ternary solar cells. Nat. Mater. *16*, 363–370.

15. Xu, X.P., Bi, Z.Z., Ma, W., Wang, Z.S., Choy, W.C.H., Wu, W.L., Zhang, G.J., Li, Y., and Peng, Q. (2017). Highly efficient ternary-blend polymer solar cells enabled by a nonfullerene acceptor and two polymer donors with a broad composition tolerance. Adv. Mater. *29*, 1704271–1704278.

16. Zhang, M., Gao, W., Zhang, F., Mi, Y., Wang, W., An, Q., Wang, J., Ma, X., Miao, J., and Hu, Z. (2018). Efficient ternary non-fullerene polymer solar cells with PCE of 11.92% and FF of 76.5%. Energy Environ. Sci. *11*, 841–849.

17. Dennler, G., Scharber, M.C., Ameri, T., Denk, P., Forberich, K., Waldauf, C., and Brabec, C.J. (2008). Design rules for donors in bulk-heterojunction tandem solar cells-towards 15

% energy-conversion efficiency. Adv. Mater. *20*, 579–583.

18. Scharber, M.C., and Sariciftci, N.S. (2013). Efficiency of bulk-heterojunction organic solar cells. Prog. Polym. Sci. *38*, 1929–1940.

19. Ameri, T., Khoram, P., Min, J., and Brabec, C.J. (2013). Organic ternary solar cells: a review. Adv. Mater. *25*, 4245–4266.

20. An, Q.S., Zhang, F.J., Zhang, J., Tang, W.H., Deng, Z.B., and Hu, B. (2016). Versatile ternary organic solar cells: a critical review. Energy Environ. Sci. *9*, 281–322.

21. Yu, R., Yao, H., and Hou, J. (2018). Recent progress in ternary organic solar cells based on nonfullerene acceptors. Adv. Energy Mater. https://doi.org/10.1002/aenm.201702814.

22. Huang, W., Cheng, P., Yang, Y.M., Li, G., and Yang, Y. (2018). High-performance organic bulk-heterojunction solar cells based on multiple-donor or multiple-acceptor components. Adv. Mater. *30*, 1705706–1705729.

23. Fu, H., Wang, Z., and Sun, Y. (2018). Advances in non-fullerene acceptor based ternary organic solar cells. Solar RRL *2*, 1700158–1700175.

24. Xiao, Z., Jia, X., and Ding, L.M. (2017). Ternary organic solar cells offer 14% power conversion efficiency. Sci. Bull. *62*, 1562–1564.

25. Ma, X., Gao, W., Yu, J., An, Q., Zhang, M., Hu, Z., Wang, J., Tang, W., Yang, C., and Zhang, F. (2018). Ternary nonfullerene polymer solar cells with efficiency >13.7% by integrating the advantages of materials and two binary cells. Energy Environ. Sci. https://doi.org/10.1039/C8EE01107A.

26. Gao, H.H., Sun, Y., Wan, X., Ke, X., Feng, H., Kan, B., Wang, Y., Zhang, Y., Li, C., and Chen, Y. (2018). A new nonfullerene acceptor with near infrared absorption for high performance ternary-blend organic solar cells with efficiency over 13%. Adv. Sci. *5*, 1800307–1800312.

27. Naveed, H.B., and Ma, W. (2018). Miscibility-driven optimization of nanostructures in ternary organic solar cells using non-fullerene acceptors. Joule *2*, 621–641.

28. Xiao, L.G., Gao, K., Zhang, Y.D., Chen, X.B., Hou, L.T., Cao, Y., and Peng, X.B. (2016). A complementary absorption small molecule for efficient ternary organic solar cells. J. Mater. Chem. A *4*, 5288–5293.

29. Lu, L.Y., Xu, T., Chen, W., Landry, E.S., and Yui, L.P. (2014). Ternary blend polymer solar cells with enhanced power conversion efficiency. Nat. Photonics *8*, 716–722.

30. Zhang, M., Zhang, F.J., An, Q.S., Sun, Q.Q., Wang, W.B., Zhang, J., and Tang, W.H. (2016). Highly efficient ternary polymer solar cells by optimizing photon harvesting and charge carrier transport. Nano Energy *22*, 241–254.

31. Wang, Z., Zhu, X., Zhang, J., Lu, K., Fang, J., Zhang, Y., Wang, Z., Zhu, L., Ma, W., Shuai, Z., et al. (2018). From alloy-like to cascade blended structure: designing high-performance all-small-molecule ternary solar cells. J. Am. Chem. Soc. *140*, 1549–1556.

32. Zhang, G.C., Zhang, K., Yin, Q.W., Jiang, X.F., Wang, Z.Y., Xin, J.M., Ma, W., Yan, H., Huang, F., and Cao, Y. (2017). High-performance ternary organic solar cell enabled by a thick active layer containing a liquid crystalline small molecule donor. J. Am. Chem. Soc. *139*, 2387–2395.

33. Xiao, L.G., Liang, T.X., Gao, K., Lai, T.Q., Chen, X.B., Liu, F., Russell, T.P., Huang, F., Peng, X.B., and Cao, Y. (2017). Ternary solar cells based on two small molecule donors with same conjugated backbone: the role of good miscibility and hole relay process. ACS Appl. Mater. Interfaces *9*, 29917–29923.

34. Li, Z.J., Xu, X.F., Zhang, W., Meng, X.Y., Genene, Z., Ma, W., Mammo, W., Yartsev, A., Andersson, M.R., Janssen, R.A.J., et al. (2017). 9.0% power conversion efficiency from ternary all-polymer solar cells. Energy Environ. Sci. *10*, 2212–2221.

35. Cheng, P., Zhang, M.Y., Lau, T.K., Wu, Y., Jia, B.Y., Wang, J.Y., Yan, C.Q., Qin, M., Lu, X.H., and Zhan, X.W. (2017). Realizing small energy loss of 0.55 eV, high open-circuit voltage >1 V and high efficiency >10% in fullerene-free polymer solar cells via energy driver. Adv. Mater. *29*, 1605216–1605221.

36. Liu, T., Guo, Y., Yi, Y.P., Huo, L.J., Xue, X.N., Sun, X.B., Fu, H.T., Xiong, W.T., Meng, D., Wang, Z.H., et al. (2016). Ternary organic solar cells based on two compatible nonfullerene acceptors with power conversion efficiency >10%. Adv. Mater. *28*, 10008–10015.

37. Bi, D.Q., Yi, C.Y., Luo, J.S., Decoppet, J.D., Zhang, F., Zakeeruddin, S.M., Li, X., Hagfeldt, A., and Gratzel, M. (2016). Polymer-templated nucleation and crystal growth of perovskite films for solar cells with efficiency greater than 21%. Nat. Energy *1*, 1–5.

38. Ma, X., Mi, Y., Zhang, F., An, Q., Zhang, M., Hu, Z., Liu, X., Zhang, J., and Tang, W. (2018). Efficient ternary polymer solar cells with two well-compatible donors and one ultranarrow bandgap nonfullerene acceptor. Adv. Energy Mater. *8*, 1702854–1702861.

39. Zhang, T., Zhao, X.L., Yang, D.L., Tian, Y.M., and Yang, X.N. (2018). Ternary organic solar cells with >11% efficiency incorporating thick photoactive layer and nonfullerene small molecule acceptor. Adv. Energy Mater. *8*, 1701691–1701699.

40. Su, W.Y., Fan, Q.P., Guo, X., Meng, X.Y., Bi, Z.Z., Ma, W., Zhang, M.J., and Li, Y.F. (2017). Two compatible nonfullerene acceptors with similar structures as alloy for efficient ternary polymer solar cells. Nano Energy *38*, 510–517.

41. Hu, Z., Zhang, F., An, Q., Zhang, M., Ma, X., Wang, J., Zhang, J., and Wang, J. (2018). Ternary nonfullerene polymer solar cells with a power conversion efficiency of 11.6% by inheriting the advantages of binary cells. ACS. Energy Lett. *3*, 555–561.

42. Yu, R.N., Zhang, S.Q., Yao, H.F., Guo, B., Li, S.S., Zhang, H., Zhang, M.J., and Hou, J.H. (2017). Two well-miscible acceptors work as one for efficient fullerene-free organic solar cells. Adv. Mater. *29*, 1700437–1700442.

43. Jiang, W.G., Yu, R.N., Liu, Z.Y., Peng, R.X., Mi, D.B., Hong, L., Wei, Q., Hou, J.H., Kuang, Y.B., and Ge, Z.Y. (2018). Ternary nonfullerene polymer solar cells with 12.16% efficiency by introducing one acceptor with cascading energy level and complementary absorption. Adv. Mater. *30*, 1703005–1703011.

44. Lin, Y., Wang, J., Zhang, Z.-G., Bai, H., Li, Y., Zhu, D., and Zhan, X. (2015). An electron acceptor challenging fullerenes for efficient polymer solar cells. Adv. Mater. *27*, 1170–1174.

45. Lin, Y.Z., Zhao, F.W., He, Q., Huo, L.J., Wu, Y., Parker, T.C., Ma, W., Sun, Y.M., Wang, C.R., Zhu, D.B., et al. (2016). High-performance electron acceptor with thienyl side chains for organic photovoltaics. J. Am. Chem. Soc. *138*, 4955–4961.

46. Lin, Y.Z., Zhang, Z.G., Bai, H.T., Wang, J.Y., Yao, Y.H., Li, Y.F., Zhu, D.B., and Zhan, X.W. (2015). High-performance fullerene-free polymer solar cells with 6.31% efficiency. Energy Environ. Sci. *8*, 610–616.

47. Liu, F., Zhou, Z.C., Zhang, C., Vergote, T., Fan, H.J., Liu, F., and Zhu, X.Z. (2016). A thieno[3,4-b] thiophene-based non-fullerene electron acceptor for high-performance bulk-heterojunction organic solar cells. J. Am. Chem. Soc. *138*, 15523–15526.

48. Qiu, N.L., Zhang, H.J., Wan, X.J., Li, C.X., Ke, X., Feng, H.R., Kan, B., Zhang, H.T., Zhang, Q., Lu, Y., et al. (2017). A new nonfullerene electron acceptor with a ladder type backbone for high-performance organic solar cells. Adv. Mater. *29*, 1604964–1604968.

49. Srivani, D., Gupta, A., Bhosale, S.V., Puyad, A.L., Xiang, W.C., Li, J.L., Evans, R.A., and Bhosale, S.V. (2017). Non-fullerene acceptors based on central naphthalene diimide flanked by rhodanine or 1,3-indanedione. Chem. Commun. *53*, 7080–7083.

50. He, B., Yang, B., Kolaczkowski, M.A., Anderson, C.A., Klivansky, L.M., Chen, T.L., Brady, M.A., and Liu, Y. (2018). Molecular engineering for large open-circuit voltage and low energy loss in around 10% non-fullerene organic photovoltaics. ACS. Energy Lett. *3*, 1028–1035.

51. Zuo, L., Shi, X., Jo, S.B., Liu, Y., Lin, F., and Jen, A.K.Y. (2018). Tackling energy loss for high-efficiency organic solar cells with integrated multiple strategies. Adv. Mater. *30*, 1706816–1706824.

52. Bi, P., Zheng, F., Yang, X., Niu, M., Feng, L., Qin, W., and Hao, X. (2017). Dual Förster resonance energy transfer effects in non-fullerene ternary organic solar cells with the third component embedded in the donor and acceptor. J. Mater. Chem. A *5*, 12120–12130.

53. Xu, W.-L., Wu, B., Zheng, F., Yang, X.-Y., Jin, H.-D., Zhu, F., and Hao, X.-T. (2015). Förster resonance energy transfer and energy cascade in broadband photodetectors with ternary polymer bulk heterojunction. J. Phys. Chem. C *119*, 21913–21920.

54. Zhang, M., Zhang, F.J., An, Q.S., Sun, Q.Q., Wang, W.B., Ma, X.L., Zhang, J., and Tang, W.H. (2017c). Nematic liquid crystal materials as a morphology regulator for ternary small molecule solar cells with power conversion efficiency exceeding 10%. J. Mater. Chem. A *5*, 3589–3598.

55. Huang, J.S., Goh, T., Li, X.K., Sfeir, M.Y., Bielinski, E.A., Tomasulo, S., Lee, M.L., Hazari,

N., and Taylor, A.D. (2013). Polymer bulk heterojunction solar cells employing Forster resonance energy transfer. Nat. Photonics *7*, 480–486.

56. Clapp, A.R., Medintz, I.L., Mauro, J.M., Fisher, B.R., Bawendi, M.G., and Mattoussi, H. (2004). Fluorescence resonance energy transfer between quantum dot donors and dye-labeled protein acceptors. J. Am. Chem. Soc. *126*, 301–310.

57. Sapsford, K.E., Berti, L., and Medintz, I.L. (2006). Materials for fluorescence resonance energy transfer analysis: beyond traditional donor–acceptor combinations. Angew. Chem. Int. Ed. *45*, 4562–4589.

58. An, Q.S., Zhang, F.J., Gao, W., Sun, Q.Q., Zhang, M., Yang, C.L., and Zhang, J. (2018). High-efficiency and air stable fullerene-free ternary organic solar cells. Nano Energy *45*, 177–183.

59. Zhao, W.C., Qian, D.P., Zhang, S.Q., Li, S.S., Inganas, O., Gao, F., and Hou, J.H. (2016). Fullerene-free polymer solar cells with over 11% efficiency and excellent thermal stability. Adv. Mater. *28*, 4734–4739.

60. Sun, C., Wu, Z.H., Hu, Z.H., Xiao, J.Y., Zhao, W.C., Li, H.W., Li, Q.Y., Tsang, S.W., Xu, Y.X., Zhang, K., et al. (2017). Interface design for high-efficiency non-fullerene polymer solar cells. Energy Environ. Sci. *10*, 1784–1791.

61. Lai, T., Xiao, L., Deng, K., Liang, T., Chen, X., Peng, X., and Cao, Y. (2018). Dimeric porphyrin small molecules for efficient organic solar cells with high photoelectron response in the near-infrared region. ACS. Appl. Mater. Interfaces *10*, 668–675.

62. Blom, P.W.M., Mihailetchi, V.D., Koster, L.J.A., and Markov, D.E. (2007). Device physics of polymer:fullerene bulk heterojunction solar cells. Adv. Mater. *19*, 1551–1566.

63. Xiao, L.G., Chen, S., Gao, K., Peng, X.B., Liu, F., Cao, Y., Wong, W.Y., Wong, W.K., and Zhu, X.J. (2016). New terthiophene-conjugated porphyrin donors for highly efficient organic solar cells. ACS Appl. Mater. Interfaces *8*, 30176–30183.

64. Cowan, S.R., Roy, A., and Heeger, A.J. (2010). Recombination in polymer-fullerene bulk heterojunction solar cells. Phys. Rev. B *82*, 245207–245216.

65. Koster, L.J.A., Mihailetchi, V.D., and Blom, P.W.M. (2006). Bimolecular recombination in polymer/fullerene bulk heterojunction solar cells. Appl. Phys. Lett. *88*, 052104–052106.